Acta Crystallographica Section D
Biological Crystallography
ISSN 0907-4449

The three-dimensional structures of two isoforms of nucleoside diphosphate kinase from bovine retina

Jane E. Ladner,[a] Najmoutin G. Abdulaev,[a,b] Dmitri L. Kakuev,[b] Mária Tordová,[a] Kevin D. Ridge[a] and Gary L. Gilliland[a]*

[a]Center for Advanced Research in Biotechnology, National Institute of Standards and Technology and the University of Maryland Biotechnology Institute, 9600 Gudelsky Drive, Rockville, MD 20850 USA, and [b]Laboratory of Light Sensitive Systems, Shemyakin and Ovchinnikov Institute of Bioorganic Chemistry, Russian Academy of Sciences, Moscow, Russia

Correspondence e-mail: gary.gilliland@nist.gov

Received 22 October 1998
Accepted 9 February 1999

PDB References: NBR-A, 1bhn; NBR-B, 1be4.

The crystal structures of two isoforms of nucleoside diphosphate kinase from bovine retina overexpressed in *Escherischia coli* have been determined to 2.4 Å resolution. Both the isoforms, NBR-A and NBR-B, are hexameric and the fold of the monomer is in agreement with NDP-kinase structures from other biological sources. Although the polypeptide chains of the two isoforms differ by only two residues, they crystallize in different space groups. NBR-A crystallizes in space group $P2_12_12_1$ with an entire hexamer in the asymmetric unit, while NBR-B crystallizes in space group $P4_32_12$ with a trimer in the asymmetric unit. The highly conserved nucleotide-binding site observed in other nucleoside diphosphate kinase structures is also observed here. Both NBR-A and NBR-B were crystallized in the presence of cGMP. The nucleotide is bound with the base in the *anti* conformation. The NBR-A active site contained both cGMP and GDP each bound at half occupancy. Presumably, NBR-A had retained GDP (or GTP) from the purification process. The NBR-B active site contained only cGMP.

1. Introduction

Photoreceptor cells embody several GTP-controlled pathways. In the retinal rod outer segment (ROS),[1] activation of the heterotrimeric guanine nucleotide-binding protein (G-protein) by photoexcited rhodopsin and GTP accounts for two crucial features of the light response: amplification and speed. It is widely accepted that the switch between the GDP-bound (inactive) and GTP-bound (active) forms of the G-protein is regulated by the GDP–GTP exchange and GTP hydrolysis by the GTP-ase activity intrinsic to G-proteins. Activated G-proteins stimulate the activity of the cyclic GMP phosophodiesterase (PDE) by relieving the inhibitory constraint of the PDE γ subunit, resulting in cGMP hydrolysis. The reduction in cGMP concentration causes the closure of plasma-membrane sodium channels gated by cGMP and subsequent rod-cell hyperpolarization (Lagnado & Baylor, 1992; Hayashi *et al.*, 1993; Koch, 1992).

The first step in the recovery of cGMP concentration is phosphorylation of GMP to GDP by guanylate kinase. In the second step, GDP is further phosphorylated to GTP by nucleoside diphosphate kinase (NDP-kinase). These two consecutive phosphotransferase reactions regulate the supply of guanine nucleotides to signal transduction and other pathways (Ruggieri & McCormick, 1991). NDP-kinase catalyzes the transfer of the γ phosphate from nucleoside

[1] Abbreviations used: ROS, rod outer segment; G-protein, guanine nucleotide-binding protein; NDP-kinase, nucleoside diphosphate kinase; PAGE, polyacrylamide gel electrophoresis; PDE, cGMP phosphodiesterase; PEG, polyethylene glycol; cGMP, cyclic 5′-guanosine monophosphate.

Table 1
Structural studies of nucleoside diphosphate kinases.

Active site	Isozyme or mutation	PDB identifier	Space group	S†	R (Å)	Reference
Bos taurus (bovine)						
cGMP/GDP	Isozyme *A*	1bhn	$P2_12_12_1$	6	2.4	This work
cGMP	Isozyme *B*	1be4	$P4_32_12$	3	2.4	This work
Dictyostelium discoideum (slime mold)						
Empty	Wild type	1npk	$P6_322$	1	1.8	Moréra, LeBras *et al.* (1994)
ADP, Mg^{2+}	Wild type	1ndp	$R3$	2	2.2	Moréra, Lascu *et al.* (1994)
Phosphorylated	Wild type	1nsp	$P6_322$	1	2.1	Moréra, Chiadmi *et al.* (1995)
2′-deoxy TDP	Wild type	1ndc	$R32$	1	2.0	Cherfils *et al.* (1994)
Empty	H122C	1ndk	$P6_322$	1	2.2	Dumas *et al.* (1992)
Empty	P105G	1ncl	$P6_322$	1	2.2	Giartosio *et al.* (1996)
Empty	P100S	1leo	$P6_322$	1	2.6	Karlsson *et al.* (1996)
ADP, AlF_3, Mg^{2+}	Wild type	1kdn	$P3_121$	3	2.0	Xu, Moréra *et al.* (1997)
AZT-DP	N119A	1lwx	$P3_121$	3	2.3	Xu, Sellam *et al.* (1997)
Drosophila melanogaster (fruit fly)						
Empty	Wild type	1ndl	$P3_221$	3	2.4	Chiadmi *et al.* (1993)
Phosphorylated	Wild type	1nsq	$P3_221$	3	2.2	Moréra, Chiadmi *et al.* (1995)
Homo sapiens (human)						
Empty	NM23-H2	1nsk	$P2_12_12_1$	6	2.8	Webb *et al.* (1995)
GDP, Mg^{2+}	NM23-H2	1nue	$P2_12_12_1$	6	2.0	Moréra, Lacombe *et al.* (1995)
Myxococcus xanthus (bacteria)						
Empty	Wild type	2nck	$P4_32_12$	2	2.0	Williams *et al.* (1993)
cAMP	Wild type	1nhk	$P4_32_12$	2	1.9	Strelkov *et al.* (1995)
ADP, Mg^{2+}	Wild type	1nlk	$P4_32_12$	2	2.0	Strelkov *et al.* (1995)

† Subunits in the asymmetric unit.

triphosphates to nucleoside diphosphates and exhibits broad specificity for the base (Parks & Agarwal, 1973). Transfer of the terminal phosphate occurs by a ping-pong mechanism which involves the formation of a transient high-energy phosphoprotein intermediate form of the enzyme arising from phosphorylation of a histidine residue, which is followed by the transfer of this phosphate to an available substrate (Parks & Agarwal, 1973; Agarwal *et al.*, 1978). The level of interest in NDP-kinases, long considered as 'housekeeping enzymes', has increased dramatically since the demonstration of their involvement in developmental processes, oncogenic transformation, tumor metastasis, apoptosis and signal transduction (for a review, see DeLaRosa *et al.*, 1995).

X-ray crystal structures are available for NDP-kinases from four different biological sources. A summary of the crystal structures is provided in Table 1. All of the structures are hexameric, except for those from the bacterium *Myxococcus xanthus* which are tetrameric. However, the fold of the monomeric unit of the enzyme and its dimeric association is consistent for all the variants. Structures have been solved with and without a nucleotide present in the active site. The nucleotide-binding site is also conserved over these widely divergent sources. The phosphate binds to the side of a β-sheet and the nucleotide base is held in a hydrophobic slot or pocket between a conserved Phe and a Val or Ile. In the hexameric form, which can be described as a trimer of dimers, there is a 23–25 Å central cavity. The major threefold interactions are at the top and bottom of this cavity and the dimeric twofold interfaces are at the equator. There are three nucleotide-binding sites on the top and three on the bottom of the hexamer. The threefold-related sites are approximately 35 Å apart, while those related by the twofold are 39 Å apart.

In a previous paper (Abdulaev *et al.*, 1998), data were presented on the purification and properties of bovine retinal NDP-kinase, the cloning of two distinct bovine retinal NDP-kinase isoforms designated NBR-A and NBR-B, and a brief account of their overall structures. It was shown that the native enzyme consists of two distinct glycosylated subunits of ~17.5 and 18.5 kDa with an apparent hexameric arrangement in solution. The enzyme is distributed along ROS disk and plasma membranes as well as in the cytoplasm. The deduced amino-acid sequences of the NBR-A and NBR-B isoforms revealed two differences: Ile21 and His135 in NBR-A are replaced by Met and Arg residues, respectively, in NBR-B. In this paper, we report a detailed description and comparison of the three-dimensional structures of the two bovine retinal NDP-kinases with bound guanine nucleotides.

2. Materials and methods

2.1. Materials

Crystallization conditions were surveyed using Crystal Screen Kits from Hampton Research.[2] Chemicals used in the final crystallizations were purchased from Sigma or Fluka. The sources of additional materials used in this investigation have been reported elsewhere (Abdulaev *et al.*, 1998).

2.2. Expression and purification of NBR-A and NBR-B NDP-kinases

Procedures for the overexpression of NBR-A and NBR-B in *Escherichia coli* and purification by $(NH_4)_2SO_4$ precipitation and chromatography on blue Sepharose CL-6B have been described previously (Abdulaev *et al.*, 1998).

2.3. Crystallization of NBR-A and NBR-B

Crystallization conditions for the two proteins were screened using Hampton Crystallization Kits I and II. The hanging-drop vapor-diffusion method was used at room temperature for all the crystallizations. After preliminary

[2] Certain commercial materials, instruments and equipment are identified in this manuscript in order to specify the experimental procedure as completely as possible. In no case does such identification imply a recommendation or endorsement by the National Institute of Standards and Technology nor does it imply that the materials, instruments or equipment identified is necessarily the best available for the purpose.

Table 2
Data and refinement statistics.

	NBR-A	NBR-B
Unique residues	Ile21, His135	Met21, Arg135
Diffraction data		
Space group	$P2_12_12_1$	$P4_32_12$
Unit-cell parameters (a, b, c) (Å)	89.9, 92.1, 131.6	128.6, 128.6, 88.2
Content of asymmetric unit	Hexamer	Trimer
V_m	2.7	3.6
Resolution limit of data (Å)	2.4	2.4
Measured intensities	165667	137791
Unique reflections	41872	30274
$R_{\rm merge}$	12.2	10.9
$R_{\rm merge}$, 2.54–2.40 Å	38.4	34.4
$I/\sigma(I)$, 2.54–2.40 Å	1.4	1.3
Observed reflections	37331	27127
Possible reflections	43409	29458
Completeness, 20.0–2.4 Å (%)	79	89
Completeness, 2.54–2.40 Å (%)	60	77
Refinement		
R factor	0.200	0.198
Number of waters	310	282
Resolution limits (Å)	20.0–2.4	20.0–2.4
Geometry: r.m.s. deviations		
Bond length (Å)	0.021	0.024
Bond angles (°)	5.13	5.53
Trigonal planes (Å)	0.024	0.022
General planes (Å)	0.026	0.025
Bad chiral centers	0	0

conditions were identified, they were optimized using customized screens close to the conditions that were identified with the kits. During the crystallization experiments, it was assumed that the GTP present in the buffer used for elution of the protein from blue Sepharose CL-6B was not high enough in concentration to remain bound to the protein after concentration with an Amicon Centricon 10 concentrator. Both proteins were concentrated to $\sim$60 mg ml^{-1} in TMED buffer containing 2 m*M* GTP. For NBR-A, screen kit 1 solution 9 provided the starting conditions. In the final conditions, the reservoir contained 100 m*M* sodium acetate buffer pH 5.0, 200 m*M* ammonium acetate and 15%(*w*/*v*) 4K polyethylene glycol. The 10 µl crystallization drops were formed by combining equal volumes of protein solution and reservoir solution. The final drop also contained 5 m*M* cGMP. The crystals were long rods which appeared in 2 d and grew to $0.1 \times 0.2 \times 0.8$ mm in 3 d. If not used immediately, the crystals redissolved within 8 d.

The final crystallization reservoir solution for NBR-B contained 100 m*M* Tris–HCl pH 7.0 and 2.3 *M* $(NH_4)_2SO_4$. The 10 µl crystallization drops were formed by combining equal volumes of protein solution and reservoir solution. The final drop also contained 2.5 m*M* cGMP. The crystals were large bipyramids which grew to $0.7 \times 0.6 \times 0.6$ mm in five months. In contrast to NBR-A, the NBR-B crystals showed no degradation with time.

2.4. X-ray data collection

Diffraction data were collected using Cu $K\alpha$ X-rays generated by a Bruker AXS rotating anode operated at 40 kV and 80 mA with a 0.3 mm collimator. A Bruker AXS Hi-Star electronic area detector was positioned at 140 mm from the crystal and at a 2θ angle of 20° for NBR-A, and at 150 mm and at a 2θ angle of 20° for NBR-B. The crystals were frozen in nylon loops in a cryo-solution made from reservoir solutions containing 20%(*v*/*v*) glycerol for NBR-A and containing 10%(*w*/*v*) PEG 8K for NBR-B. The high salt NBR-B crystals dissolved when glycerol was used as a cryo-protectant. During data collection, the crystals were maintained at 100 K in a nitrogren cold stream by an Oxford Cryosystems Cryostream. Diffraction data were processed with *XENGEN* (Howard *et al.*, 1987). Table 2 provides a summary of the diffraction data statistics.

2.4.1. Structure solution. The structures were solved by molecular replacement using the *AMoRe* program (Navaza, 1994) from the *CCP*4 package (Collaborative Computational Project, Number 4, 1994). Of the NDP-kinases for which there are structures available, the sequence homology is highest between bovine and human NM23-H2. We chose to work on the NBR-B structure first because the asymmetric unit is smaller. For NBR-B, a trimer from the human recombinant NM23-H2 structure (Webb *et al.*, 1995), 1nsk (Protein Data Bank code; Bernstein *et al.*, 1977) was used as the search structure. This unligated structure was the coordinate set which we had available when we began the project. Although there are 15 sequence changes in the monomer when going from human NM23-H2 to bovine NBR-B, the human sequence was retained during the molecular-replacement procedures. The *AMoRe* program gave three rotational solutions which were threefold related and three times more significant than any other solutions for NBR-B. The diffraction data indicated that the space group is $P4_12_12$ or $P4_32_12$. The translation function unambiguously showed that the space group was $P4_32_12$. The final *AMoRe* solution gave an R factor of 0.32 for the rigid-body rotated and translated structure.

For the NBR-A structure, a complete hexamer was generated from the NBR-B structure and this was used as a search structure in *AMoRe* without altering the sequence at positions 21 and 135. Six related rotational solutions were obtained which were four times as significant as any other solutions. *AMoRe* found a translation solution which gave an R value of 0.38. The final rigid-body solution from *AMoRe* had an R value of 0.32 over the resolution range 20.0–3.4 Å.

The molecular display and map-fitting program, *TURBO FRODO* (Roussel *et al.*, 1996), was used to change the model to the proper primary sequence for NBR-B and NBR-A and subsequently to examine and adjust the structures during the refinement process.

A combination of the refinement programs *X-PLOR* (Brünger, 1992) and *TNT* (Tronrud *et al.*, 1987) was used to refine the atomic positions and thermal factors. *X-PLOR* was used to perform simulated-annealing, slow-cooling, positional and B-factor (temperature-factor) refinement. During this procedure no ligands or waters were included. For NBR-B, 10% of the data was used for calculation of $R_{\rm free}$ during the refinement with *X-PLOR* and $R_{\rm free}$ fell from 0.398 to 0.366; the working R factor at the end of the *X-PLOR* refinement was 0.259. For the NBR-A refinement, $R_{\rm free}$ was not followed. *TNT*

was then used to include the ligands and waters. The final refinement statistics for both NBR-A and NBR-B are shown in Table 2. The non-crystallographic symmetry option was used as a restraint during the *TNT* refinements. For the NBR-B structure, where the non-crystallographic symmetry is threefold, the weight of the restraint was decreased from 30 to 0 during the refinement. For the NBR-A structure, where the non-crystallographic symmetry is sixfold, the weight was decreased to 10 during the refinement, and during the final cycles was maintained only for atoms in the hydrophobic core of the molecule. The solvent structures were solved independently by using the peak-picking facility in *TNT* and by observation when visually examining the $F_o - F_c$ difference maps in *TURBO FRODO*. Positions were selected for water molecules when the difference density was greater than 3σ and the environment was appropriate for a water molecule. Subsequently, solvent molecules were deleted from the coordinates if the *B* value became greater than 90 or the $2F_o - F_c$ density was significantly below 1σ. The nucleotide density was easily seen in the first electron-density maps. In NBR-B, the cGMP starting structure, adapted from the cAMP in the *M. xanthus* NDP-kinase structure, 1nhk (Strelkov *et al.*, 1995), fitted well. In NBR-A, although the cGMP fitted well, there was extra density in the phosphate region which was found to fit the GDP structure from 1nue (Moréra, Lacombe *et al.*, 1995). Since cGMP was present, it was not possible to determine whether the second nucleotide was GDP or GTP; the third phosphate of GTP would coincide with the phosphate from cGMP. In the final model, cGMP and GDP were included each at half occupancy in NBR-A.

The program *PROCHECK* (Laskowski *et al.*, 1993) was used to examine the stereochemical parameters of the final structures. These structures were compared with other NDP-kinase structures using *ALIGN* (Satow *et al.*, 1986) and *TURBO FRODO* (Roussel *et al.*, 1996) to align the coordinate files and examine the results.

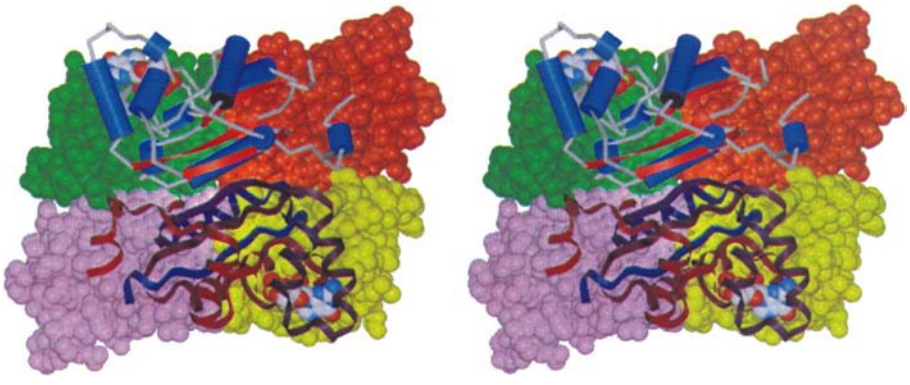

Figure 1
Stereoview of the NBR-A hexamer. Chains *B*, *C*, *D* and *F* are shown as space-filling models with each chain a different color. The fold of the *A* monomer is shown with helices represented by blue cylinders and β-sheets represented by red ribbons. Chain *E* is represented by a ribbon with the color changing from blue at the N-terminus to red at the C-terminus. Space-filling models of cGMP are shown in the active sites of the *A* and *E* chains. This figure was generated using *TkRaster3D*, a graphical user interface developed by Hillary S. R. Gilson at the National Institute of Standards and Technology for the molecular-rendering package *Raster3D* (Bacon & Anderson, 1988; Merritt & Murphy, 1994).

2.4.2. Other Methods. The NDP-kinase spectrophotometric assay, equilibrium sedimentation and electrophoretic analysis were all performed as described (Abdulaev *et al.*, 1998).

3. Results

3.1. Purification and properties of NBR-A and NBR-B NDP-kinases

3.1.1. Purification of NBR-A and NBR-B NDP-kinases. The purification protocol for retinal NDP-kinase (Abdulaev *et al.*, 1998), with a slight modification, was successfully adapted for the preparation of recombinant NDP-kinase expressed in *E. coli*. Typically, 18–20 mg of purified NBR-A and NBR-B were obained from a 500 ml shake-flask culture. The specific activity of NBR-A was ~857 units mg^{-1}, while that for NBR-B was ~1063 units mg^{-1}. For comparison, only ~1 mg of purified NDP-kinase could be isolated from 200 retinae, and the resulting enzyme exhibits a specific activity of ~763 units mg^{-1} protein (Abdulaev *et al.*, 1998). Although the K_m values of the NBR-A and NBR-B enzymes for either ATP or GTP were similar, they were three to five times lower than observed for retinal NDP-kinase. Further, while either CDP or TDP served equally well as acceptor substrates for retinal NDP-kinase and NBR-A, TDP was clearly the preferred substrate over CDP for NBR-B.

3.1.2. Properties of NBR-A and NBR-B NDP-kinases. The deduced amino-acid sequences for NBR-A and NBR-B encode proteins of 17262 and 17299 Da, respectively (Abdulaev *et al.*, 1998). This slight difference in molecular weight is a consequence of the substitution of Ile21 and His135 in NBR-A for Met and Arg, respectively, in NBR-B. NBR-A and NBR-B each showed a single polypeptide chain of ~17 kDa on SDS–PAGE. Bovine retinal NDP-kinase, like several other NDP-kinases (Presecan *et al.*, 1989; Kimura & Shimada, 1988; Nickerson & Well, 1984), migrates on SDS–PAGE as a closely spaced doublet of 17.5 and 18.5 kDa (Abdulaev *et al.*, 1998). Similar to retinal NDP-kinase, the isoelectric focusing patterns of NBR-A and NBR-B show six to seven major protein bands. However, the p*I* range for NBR-A was 8.0–8.5 while that for NBR-B was 6.5–7.5. Sedimentation equilibrium of NBR-A and NBR-B showed absolute molecular masses of 97 and 95 kDa, respectively. This is suggestive of a hexameric arrangement for the enzyme, which is characteristic of many eukaryotic NDP-kinases (Yue *et al.*, 1967; Palmieri *et al.*, 1973; Presecan *et al.*, 1989; Gilles *et al.*, 1991; Lascu *et al.*, 1992; Hamby *et al.*, 1995; Schaertl, 1996).

3.1.3. Overall structure of NBR-A and NBR-B kinases. A stereoview of an NBR-A hexamer is shown in Fig. 1. The

Table 3
R factor as a function of resolution.

Bragg spacing (Å)	NBR-A		NBR-B	
	Reflections	*R* factor	Reflections	*R* factor
6.44	4492	0.21	3094	0.21
4.50	4174	0.14	2903	0.13
3.80	3934	0.15	2817	0.14
3.40	3566	0.18	2742	0.17
3.13	3418	0.21	2660	0.21
2.93	3257	0.24	2582	0.24
2.77	3051	0.25	2546	0.26
2.64	3018	0.27	2427	0.28
2.53	2711	0.30	2353	0.30
2.44	2581	0.29	2194	0.31
Total	34202	0.200	26318	0.198

final coordinates for NBR-A includes 906 amino acids (151 per monomer), six cGMP ligands and six GDP ligands (each at half occupancy) and 310 solvent molecules. The overall quality of the $2F_o - F_c$ electron density is quite good. The $F_o - F_c$ difference peaks for the ligands and for the sequence change Met21→Ile21 when going from NBR-B to NBR-A were quite clear. However, the final electron density is of poor quality in the region of residues 52–58 and at the N-terminus residues Ala2 and Asn3. In a Ramachandran plot (Ramachandran & Sasisekharan, 1968), 82.2% of the non-glycine and non-proline residues are in the most-favored regions (Fig. 2). 11 residues are in the generously allowed region and none are in the disallowed regions. Six of the 11 residues in the generously allowed region are Ile116 from each chain. In all published NDP-kinase structures, the residue at this position is in a strained conformation. The variation of the *R* factor is shown as a function of resolution in Table 3.

The final model for NBR-B includes 453 amino-acid residues (residues 2–152), three cGMP ligands and 282 solvent molecules. The overall quality of the electron density is good. The electron density for the ligands was well defined with no evidence of GDP. However, the electron-density level is low for residues 53–60 and for the N-terminal residue Ala2, and no electron density is observed for Met1. Hence, it is not included in the structure. In a Ramachandran plot, 83.1% of the non-glycine and non-proline residues are in the most-favored regions (Fig. 2). Eight residues are in the generously allowed region and none are in the disallowed regions. Two of the eight residues in the generously allowed region are Ile116 from chains *A* and *C*.

The three-dimensional structures of NBR-A and NBR-B are very similar to each other and to published structures for other hexameric NDP-kinases from different biological sources. The r.m.s. difference of the C^{α} positions for the trimer of NBR-B to the two trimers in NBR-A are 0.48 and 0.47 Å. The monomer folds into a compact structure with a core of antiparallel β-sheet partially covered by α-helices, as shown in Fig. 1. The residues 53–58 form a boundary for the nucleotide-binding pocket. The region which includes residues 93–115 is referred to as the Kpn loop in reference to a *Drosophila* mutant. The sequence in this region is strictly conserved between the human and bovine molecules and highly conserved between the bovine and *Drosophila* molecules. The Kpn loop is involved in the most significant trimeric contacts. The C-terminal regions form a ring around the structure. The C-terminal residue Glu152 defines the edge of the nucleotide pocket of its neighbor in the trimer.

There are only two residues which are different between NBR-A and NBR-B. Position 21 is Ile in NBR-A and Met in NRB-B, while position 135 is His in NBR-A and Arg in NBR-B. Residue 21 is on the interior of the molecule and is part of a hydrophobic region which forms the dimer interface. Position

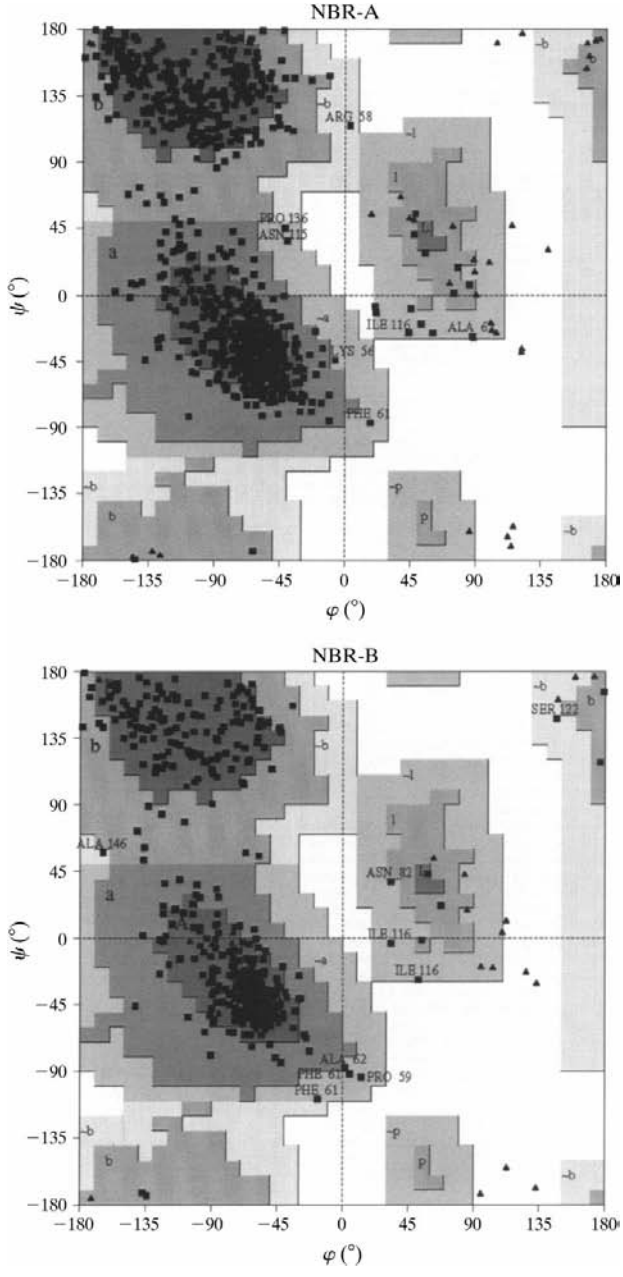

Figure 2
The Ramachandran plots for the NBR-A and NBR-B structures. These plots were generated by *PROCHECK* (Laskowski *et al.*, 1993). Gly residues are represented by triangles and all other residues are represented by squares.

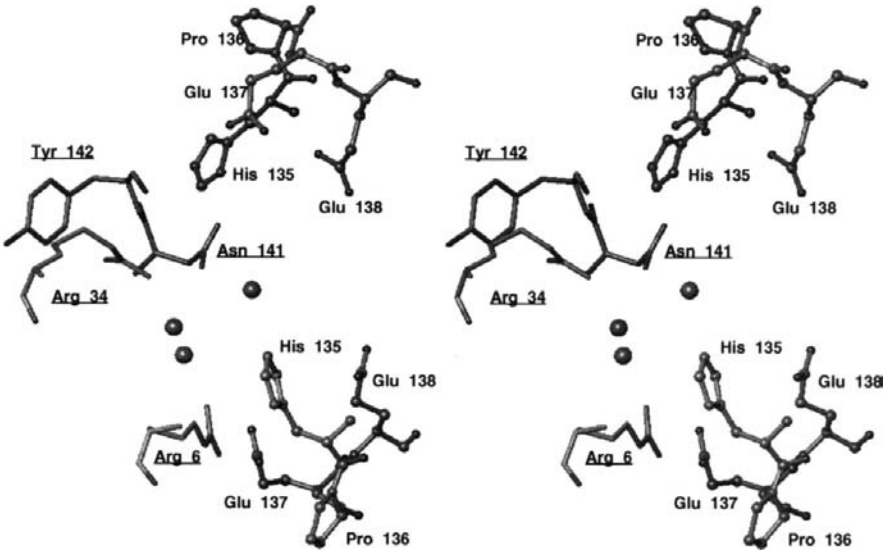

Figure 3
A stereoview of a crystal contact in NBR-A. Chain *C* (upper right) and chain *E* (lower right) of one hexamer are positioned above and below residue Asn141 of a crystallographic neighboring hexamer. The residue labels in the neighboring macromolecule are underlined. The distance from C^{α} His135 chain *A* to C^{α} His135 chain *E* is 17 Å. This figure was generated in *TURBO FRODO* (Roussel *et al.*, 1996).

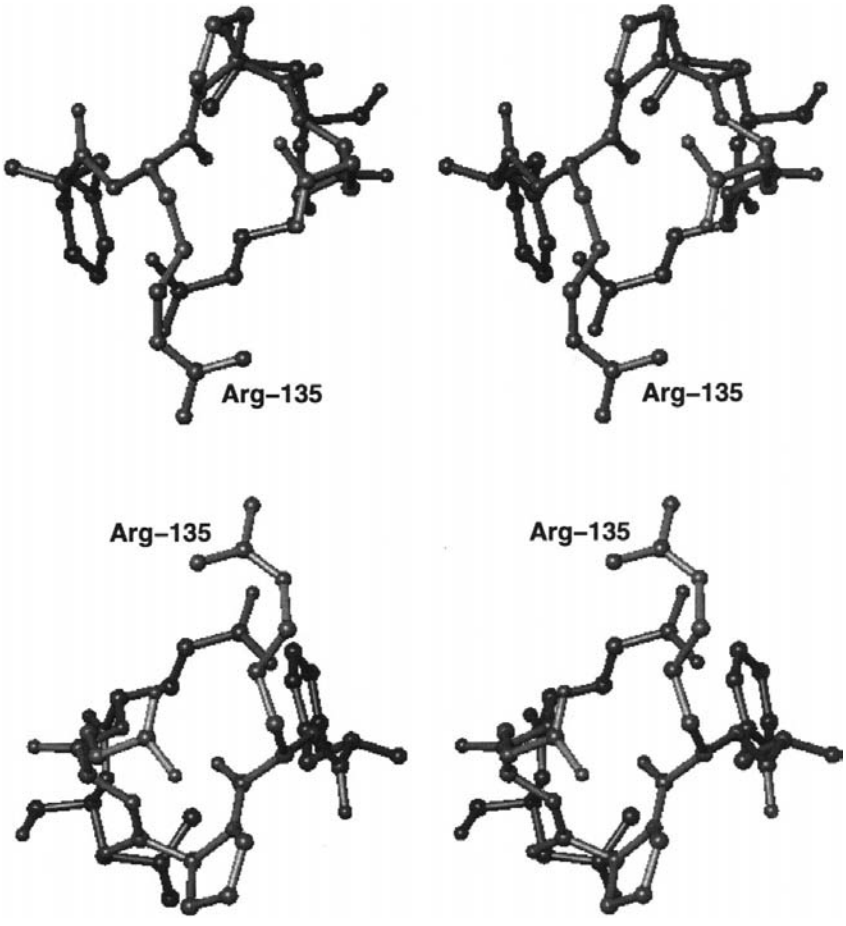

Figure 4
A stereoview of a crystal contact in NBR-B. The twofold contact between Arg135 $N^{\eta 2}$ of chain *C* of one trimer and Arg135 $N^{\eta 2}$ chain *C* of the crystallographically related trimer is 3.0 Å. This figure was generated in *TURBO FRODO* (Roussel *et al.*, 1996).

135 is on the exterior of the molecule. In the orthorhombic form, NBR-A, His135 in chain *E* is involved in an intermolecular contact with Asn141 from chain *D* of another molecule (Fig. 3). In the tetragonal crystal form, NBR-B, these contacts are not present. However, as shown in Fig. 4, the side chains of the Arg135 residues are involved in crystal contacts. In the *C* chain, the dyad-related side chains approach to within 3.0 Å.

3.1.4. Nucleotide-binding site. The nucleotide-binding sites of NBR-A and NBR-B are very similar to those described for other NDP-kinases. The nucleotide base is stacked face-to-face with Phe60 and Val112 is on the opposite side. Both of these residues are conserved across species with only one exception. In *M. xanthus*, the position equivalent to 112 is Ile. The polar contacts are summarized in Table 4, showing the average of the distances observed in this study for the three active sites of NBR-B and for the six active sites of NBR-A. A view of the NBR-B active site is shown in Fig. 5. The $2F_o - F_c$ maps of representative active sites for both NBR-A and NBR-B are shown in Fig. 6.

3.1.5. Solvent structure. In NBR-A, 225 of the 310 waters (73%) are in the first hydration sphere. In NBR-B, 214 of the 282 waters (76%) are in the first hydration sphere. When the solvent structures are compared by superimposing NBR-B and its twofold crystallographic mate on the NBR-A hexamer, there are 82 water positions which agree to within 1.0 Å.

3.1.6. Comparison with other NDP-kinase structures. The C^{α} trace of a trimer of NBR-B with monomers from the structures of NDP-kinases from three different biological sources superimposed is shown in Fig. 7. The largest differences are in the C-termini and in residues 53–58. At least part of the observed movement in this region in the comparison with *D. melanogaster* is attributable to the binding of the nucleotide in the active site, since that structure has an empty active site.

4. Discussion

The NBR-A and NBR-B enzymes differ from each other and from retinal NDP-kinase in enzymatic properties, isoelectric point and/or electrophoretic behavior. A

Table 4
Contacts between protein and nucleotide.

Protein atom	cGMP atom	NBR-A average distance (Å)	NBR-B average distance (Å)	GDP atom	NBR-A average distance (Å)
Lys12 N^{ζ}	O1A	3.2	2.6		
Lys12 N^{ζ}	O3*	3.1	3.5	O3*	3.2
Lys12 N^{ζ}	O2*	3.1	2.9	O2*	3.3
Tyr52 OH	O1A	2.7	3.0		
Arg88 $N^{\eta 2}$				OB1	3.4
Arg88 $N^{\eta 2}$				OB2	3.3
Thr94 $O^{\gamma 1}$				O3A	3.4
Val112 O	O2*	3.4	3.6	O2*	3.1
Asn115 $N^{\delta 2}$	O3*	3.6	3.6	O3*	3.1
Asn115 $O^{\delta 1}$	O2*	3.6	3.2	O2*	3.6
His118 $N^{\delta 1}$	O2A	3.2	2.8	O2A	3.2
His118 $N^{\delta 1}$	O1A	3.0	3.4		
His118 $N^{\delta 1}$	O2A	3.2	2.8	O2A	3.2
Glu152 $O^{\varepsilon 1}$	N2	3.7	2.9		
Glu152 $O^{\varepsilon 2}$		3.6			

goal of the present investigation was to discern whether there was a structural basis for some of these biochemical differences. As noted, the only differences in amino-acid composition between NBR-A and NBR-B are at positions 21 and 135. Position 21 is on the interior of the molecule and is part of the region which forms the dimer interface, while residue 135 is on the exterior of the molecule near the twofold interface. Therefore, it is highly unlikely that these residues account for the observed difference in enzymatic properties between NBR-A and NBR-B. Additionally, since the exact polypeptide or amino-acid composition of the retinal NDP-kinase hexamer is not known, it is also difficult to rationalize the observed differences in the K_m values for the different nucleoside diphosphate and triphosphate substrates from those of the NBR-A and NBR-B isoforms.

Both NBR-A and NBR-B showed a single polypeptide chain of ~17 kDa on SDS–PAGE while the native enzyme, like several other NDP-kinases (Presecan *et al.*, 1989; Kimura & Shimada, 1988; Nickerson & Well, 1984), migrates as a closely spaced doublet of 17.5 and 18.5 kDa. This difference may be attributed to various post-translational modifications of retinal NDP-kinase. We have shown that the N-terminal amino acid on retinal NDP-kinase is blocked and that the enzyme contains ~2–3%(*w*/*w*) carbohydrate (Abdulaev *et al.*, 1998). Although the N-terminal Met is not included in the structures reported here, Ala2 is on the surface of the mole-

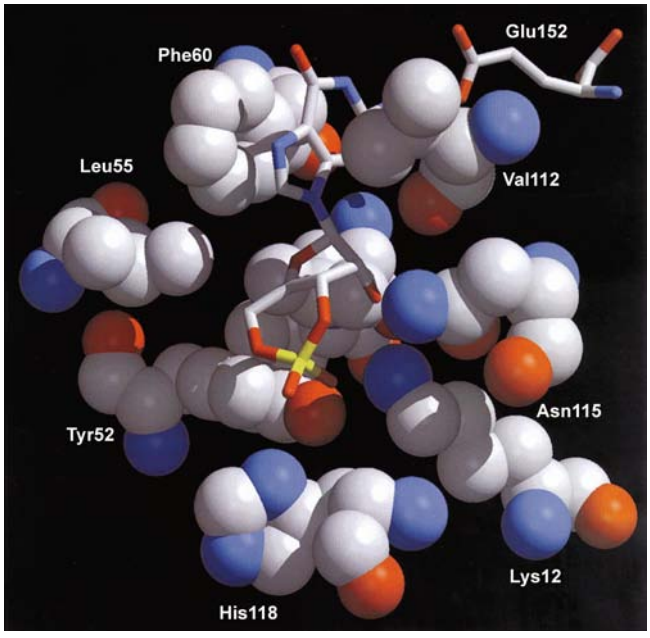

Figure 5
The active site of NBR-B. The chain *C* residues near the active site are represented as space-filling models with radii 70% of the van der Waals radii. The cGMP molecule and chain *A* Glu152 are represented as stick models. This figure was generated using *TkRaster3d* (Bacon & Anderson, 1988; Merritt & Murphy, 1994).

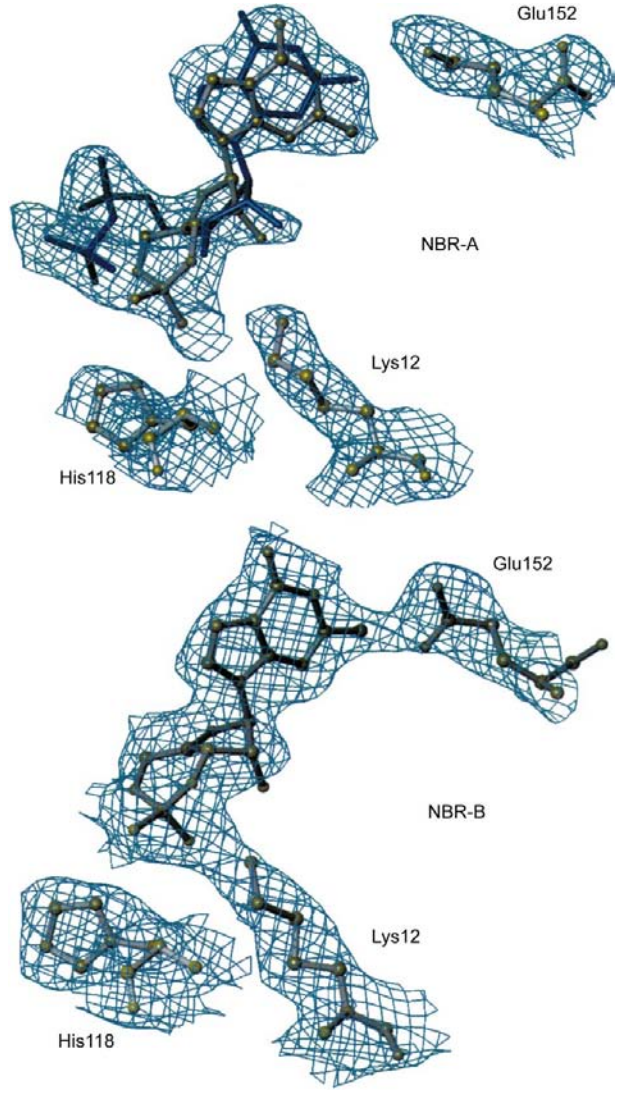

Figure 6
The $2F_o - F_c$ density for the nucleotide and active-site residues of NBR-A and NBR-B. In both representations, the nucleotide ligands, Lys12 and His118 are from chain *C* and Glu152 is from chain *A*. In NBR-A, the licorice model is GDP and the ball-and-stick model is cGMP. The NBR-A map is contoured at 0.85σ. In the NBR-B map, the contour level is 1.0σ. Both figures were generated in *TURBO FRODO* (Roussel *et al.*, 1996).

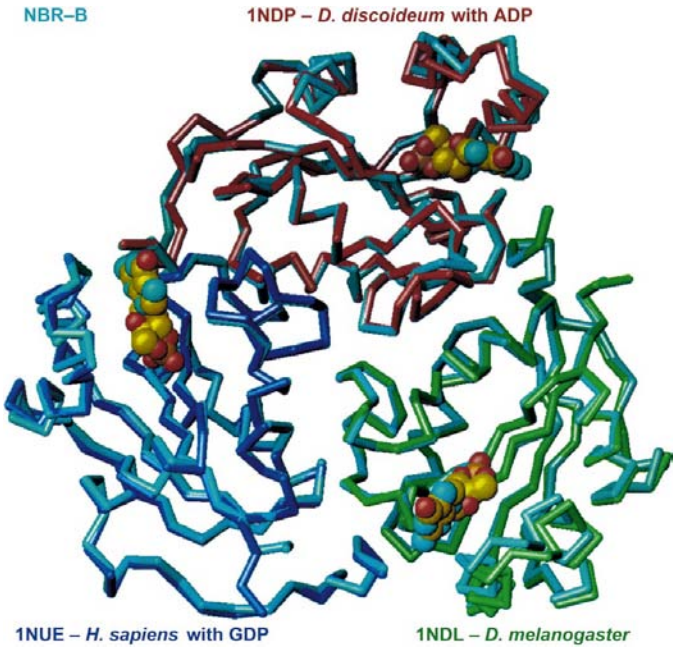

Figure 7
Superposition of monomers from NDP-kinases from other biological sources on the trimer from NBR-B. The figure was generated in *TURBO FRODO* (Roussel *et al.*, 1996).

cule. The potential glycosylation sites Glu–Arg–Thr–Phe (amino-acid residues 5–8) and Val–Lys–Thr–Gly (amino-acid residues 84–87) are also on the exterior of the molecule and are readily accessible for modification by glycosylation enzymes. These sites are adjacent to each other and the distance between the C^{α} of Glu5 and the C^{α} of Val84 is 7 Å. Like the retinal enzyme, the isoelectric focusing pattern of NBR-A and NBR-B shows six to seven major protein bands. This is consistent with the existence of different oligomeric species and/or the extent of phosphorylation within these oligomers. However, the p*I* ranges of NBR-A and NBR-B differ from each other (8.0–8.5 and 6.5–7.5, respectively) and from that of retinal NDP-kinase (7.4–8.2). For NBR-A and NBR-B, this difference is presumably due to the amino acid at position 135. It is possible that this charge difference may also influence the phosphorylation state of the protein. As indicated above, since the exact amino-acid or polypeptide composition of a retinal NDP-kinase hexamer is not known, it is difficult to explain the difference in p*I* from the NBR-A and NBR-B isoforms.

The nucleotide-binding sites in the bovine retinal structures agree with the now well established active site defined for *D. discoideum*, human NM23-H2, *D. melanogaster* and *M. xanthus*. All residues in the active site are highly conserved. Six residues which form polar interactions with either the ribose or the phosphates in cGMP and GDP are strictly conserved in the NDP-kinases. These residues are Lys12, Tyr52, Arg88, Thr94, His118 and Asn115. The site does not discriminate between the various bases, since the principal interaction with the base is hydrophobic stacking. The nucleotide base is positioned between the strictly conserved Phe60 and Val112. Val112 is conserved in all known NDP-kinases, with the exception of *M. xanthus* where it is replaced by Ile. Structures of other NDP-kinases have been solved with adenine, thymine and guanine nucleotide phosphates. The interaction with the C-terminal residue can be through a water for the smaller bases. The solved structures have also included a variety of phosphate and ribose moieties: 5′-cyclic phosphate, diphosphate, ribose and deoxyribose. The other NDP-kinase structure solved with a cyclic nucleotide in the active site was the tetrameric form, 1nhk, where the nucleotide base was observed to be in both the *syn* and *anti* conformations. In the two bovine structures, only the *anti* conformer was observed. This is probably a consequence of the interactions of N6 of the guanosine base with Glu152 of the neighboring monomer. The tetrameric *M. xanthus* NDPK is missing the terminal six residues and does not form the trimeric interaction which brings the carboxy-terminus of one chain adjacent to the active site of the neighboring chain of the trimer. Thus, the nucleotide base is not anchored in the *anti* conformation in this structure as it is in the hexameric bovine structures.

This work was supported in part by a grant from the International Science Foundation and by NIST. We would like to thank J. Fujiwara for technical assistance and T. Ngo for assistance in preparing the manuscript.

References

Abdulaev, N. G., Karaschuk, G. N., Ladner, J. E., Kakuev, D. L., Yakhyaev, A. V., Tordova, M., Gaidarov, I. O., Popov, V. I., Fujiwara, J. H., Chinchilla, D., Eisenstein, E., Gilliland, G. L. & Ridge, K. D. (1998). *Biochemistry*, **37**, 13958–13967.
Agarwal, R. P., Robison, B. & Parks, R. E. Jr (1978). *Methods Enzymol.* **51**, 376–386.
Bacon, D. J. & Anderson, W. F. (1988). *J. Mol. Graph.* **6**, 219–220.
Bernstein, F. C., Koetzle, T. F., Williams, G. J. B., Meyer, E. F. Jr, Brice, M. D., Rogers, J. R., Kennard, O., Shimanouchi, T. & Tasumi, M. (1977). *J. Mol. Biol.* **112**, 535–542.
Brünger, A. T. (1992). *X-PLOR Version* 3.1. *A System for X-ray Crystallography and NMR*. New Haven, CT: Yale University Press.
Cherfils, J., Moréra, S., Lascu, I., Véron, M. & Janin, J. (1994). *Biochemistry*, **33**, 9062–9069.
Chiadmi, M., Moréra, S., Lascu, I., Dumas, C., LeBras, G., Véron, M. & Janin, J. (1993). *Structure*, **1**, 283–293.
Collaborative Computational Project, Number 4 (1994). *Acta Cryst.* D**50**, 760–763.
DeLaRosa, A., Williams, R. L. & Steeg, P. S. (1995). *Bioessays*, **17**, 53–62.
Dumas, C., Lascu, I., Moréra, S., Glaser, P., Fourme, R., Wallet, V., Lacombe, M.-L., Véron, M. & Janin, J. (1992). *EMBO J.* **11**, 3203–3208.
Giartosio, A., Erent., M., Cervoni, L., Moréra, S., Janin, J., Konrad, M. & Lascu, I. (1996). *J. Biol. Chem.* **271**, 17845–17851.
Gilles, A.-M., Presecan, E., Vonica, A. & Lascu, I. (1991). *J. Biol. Chem.* **266**, 8784–8789.
Hamby, C. V., Mendola, C. E., Potla, L., Stafford, G. & Backer, J. M. (1995). *Biochem. Biophys. Res. Commun.* **211**, 578–585.
Hayashi, F., Hutson, L. D., Kishigami, A., Nagao, S. & Yamazaki, A. (1993). *Methods Neurosci.* **15**, 237–247.
Howard, A., Gilliland, G. L., Finzel, B. C., Poulos, T. L., Ohlendorf, D. H. & Salemme, F. R. (1987). *J. Appl. Cryst.* **20**, 383–387.

Karlsson, A., Mesnildrey, S., Xu, Y., Moréra, S., Janin, J. & Véron, M. (1996). *J. Biol. Chem.* **271**, 19928–19934.
Kimura, N. & Shimada, N. (1988). *J. Biol. Chem.* **263**, 4647–4653.
Koch, K.-W. (1992). *Trends Biochem. Sci.* **17**, 307–311.
Lagnado, L. & Baylor, D. (1992). *Neuron*, **8**, 995–1002.
Lascu, I., Chaffotte, A., Limbourg-Bouchon, B. & Veron, M. (1992). *J. Biol. Chem.* **267**, 12775–12781.
Laskowski, R. A., MacArthur, M. W., Moss, D. S. & Thornton, J. M. (1993). *J. Appl. Cryst.* **26**, 283–291.
Merritt, E. A. & Murphy, M. E. P. (1994). *Acta Cryst.* D**50**, 869–873.
Moréra, S., Chiadmi, M., LeBras, G., Lascu, I. & Janin, J. (1995). *Biochemistry*, **34**, 11062–11070.
Moréra, S., Lacombe, M.-L., Yingwu, X., LeBras, G. & Janin, J. (1995). *Structure*, **3**, 1307–1314.
Moréra, S., Lascu, I., Dumas, C., LeBras, G., Briozzo, P., Véron, M. & Janin, J. (1994). *Biochemistry* **33**, 459–467.
Moréra, S., LeBras, G., Lascu, I., Lacombe, M. L., Véron, M. & Janin, J. (1994). *J. Mol. Biol.* **243**, 873–890.
Navaza, J. (1994). *Acta Cryst.* A**50**, 157–163.
Nickerson, J. A. & Well, W. W. (1984). *J. Biol. Chem.* **259**, 11297–11304.
Palmieri, R., Yue, R. H., Jacobs, H. K., Maland, L., Wu, L. & Kuby, S. A. (1973). *J. Biol. Chem.* **248**, 4486–4499.
Parks, R. E. & Agarwal, R. P. (1973). *The Enzymes*, edited by P. D. Boyer, Vol. 8, pp. 307–333. New York: Academic Press.
Presecan, E., Vonica, A. & Lascu, I. (1989). *FEBS Lett.* **250**, 629–632.
Ramachandran, G. N. & Sasisekharan, V. (1968). *Adv. Protein Chem.* **23**, 283–438.
Roussel, A., Inisan, A.-G. & Cambillau, C. (1996). *TURBO FRODO*. AFMB and BioGraphics, Marseille, France.
Ruggieri, R. & McCormick, F. (1991). *Nature (London)*, **353**, 390–391.
Satow, Y., Cohen, G. H., Padlan, E. A. & Davies, D. R. (1986). *J. Mol. Biol.* **190**, 593–604.
Schaertl, S. (1996). *FEBS Lett.* **394**, 316–320.
Strelkov, S. V., Perisic, O., Webb, P. A. & Williams, R. L. (1995). *J. Mol. Biol.* **249**, 665–674.
Tronrud, D., Ten Eyck, L. & Matthews, B. W. (1987). *Acta Cryst.* A**43**, 489–501.
Webb, P. A., Perisic, O., Mendola, C. E., Backer, J. M. & Williams, R. L. (1995). *J. Mol. Biol.* **251**, 574–587.
Williams, R. L., Oren, D. A., Muñoz-Dorado, J., Inouye, S., Inouye, M. & Arnold, E. (1993). *J. Mol. Biol.* **234**, 1230–1247.
Xu, Y.-W., Moréra, S., Janin, J. & Cherfils, J. (1997). *Proc. Natl Acad. Sci. USA*, **94**, 3579–3583.
Xu, Y.-W., Sellam, O., Moréra, S., Sarfati, S., Biondi, R., Véron, M. & Janin, J. (1997). *Proc. Natl Acad. Sci. USA*, **94**, 7162–7165.
Yue, R. H., Ratliff, R. L. & Kuby, S. A. (1967). *Biochemistry*, **6**, 2923–2932.